

Theory of electronic states and transport in carbon nanotubes

Tsuneya Ando

Department of Physics, Tokyo Institute of Technology, 2-12-1 Ookayama, Meguro-ku, Tokyo 152-8551, Japan

Abstract. A brief review is given of electronic and transport properties of carbon nanotubes mainly from a theoretical point of view. The topics cover an effective-mass description of electronic states, optical absorption including interaction effects on the band gap and excitonic effects, and the absence of backward scattering except for scatterers with a potential range smaller than the lattice constant which causes a metallic nanotube to be a ballistic conductor even at room temperature.

1. Introduction

Carbon nanotubes (CNs) are quasi-one-dimensional materials made of sp^2 -hybridized carbon networks [1] and have been a subject of an extensive study. In particular, the electronic structure of a single CN has been studied theoretically, which predicted that CN becomes either metallic or semiconducting depending on its chiral vector, i.e., boundary conditions in the circumference direction. [2, 3, 4, 5, 6, 7, 8, 9, 10, 11]. These predictions have been confirmed by Raman experiments [12] and direct measurements of local density of states by scanning tunneling spectroscopy [13, 14, 15]. The purpose of this paper is to give a brief review of recent theoretical study on electronic and transport properties of carbon nanotubes.

Transport properties are particularly interesting because of their unique topological structures [16]. For potential scattering, it was shown theoretically that there is no backscattering for impurity potentials with a range larger than the lattice spacing in metallic CNs [17]. The absence of backscattering was related to Berry's phase acquired by a rotation in the wave-vector space in the system described by a $\mathbf{k}\cdot\mathbf{p}$ Hamiltonian [18]. It has been confirmed by numerical calculations in a tight-binding model [19]. There have been some reports on experiments which seem to support this theoretical prediction [20, 21].

In understanding electronic properties of nanotubes, a $\mathbf{k}\cdot\mathbf{p}$ method or an effective-mass approximation [11] has been quite useful. It has been used successfully in the study of wide varieties of electronic properties of CN. Some of such examples are magnetic properties [22] including the Aharonov-Bohm effect on the band gap, optical absorption spectra [23], exciton effects [24], lattice instabilities in the absence [25, 26] and presence of a magnetic field [27], magnetic properties of ensembles of nanotubes [28], effects of spin-orbit interaction [29], effects of lattice vacancies [30, 31], and electronic properties of nanotube caps [32]. In this paper, we shall first discuss electronic states, then optical spectra, and finally transport properties, obtained mainly in the $\mathbf{k}\cdot\mathbf{p}$ scheme.

2. Energy bands

Figure 1 shows the lattice structure and the first Brillouin zone of a two-dimensional (2D) graphite together with the coordinate systems. The unit cell contains two carbon atoms

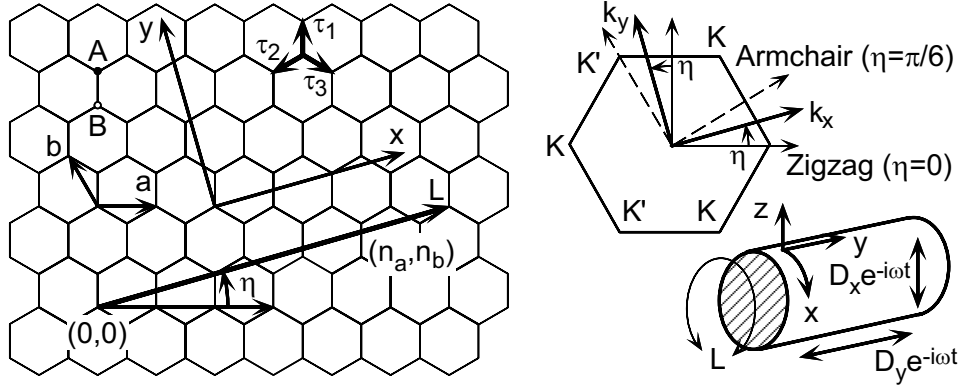


Figure 1. (a) Lattice structure of two-dimensional graphite sheet. η is the chiral angle. The coordinates are chosen in such a way that x is along the circumference of a nanotube and y is along the axis. (b) The first Brillouin zone and K and K' points. (c) The coordinates for a nanotube.

denoted by A and B. A nanotube is specified by a chiral vector $\mathbf{L} = n_a \mathbf{a} + n_b \mathbf{b}$ with integer n_a and n_b and basis vectors \mathbf{a} and \mathbf{b} ($|\mathbf{a}| = |\mathbf{b}| = a = 2.46 \text{ \AA}$). In the coordinate system fixed onto a graphite sheet, we have $\mathbf{a} = (a, 0)$ and $\mathbf{b} = (-a/2, \sqrt{3}a/2)$. For convenience we introduce another coordinate system where the x direction is along the circumference \mathbf{L} and the y direction is along the axis of CN. The direction of \mathbf{L} is denoted by the chiral angle η .

A graphite sheet is a zero-gap semiconductor in the sense that the conduction and valence bands consisting of π states cross at K and K' points of the Brillouin zone, whose wave vectors are given by $\mathbf{K} = (2\pi/a)(1/3, 1/\sqrt{3})$ and $\mathbf{K}' = (2\pi/a)(2/3, 0)$ [33]. Electronic states near a K point of 2D graphite are described by the $\mathbf{k} \cdot \mathbf{p}$ equation [11, 34]:

$$\gamma(\vec{\sigma} \cdot \hat{\mathbf{k}})\mathbf{F}^K(\mathbf{r}) = \varepsilon \mathbf{F}^K(\mathbf{r}), \quad \mathbf{F}^K(\mathbf{r}) = \begin{pmatrix} F_A^K(\mathbf{r}) \\ F_B^K(\mathbf{r}) \end{pmatrix}, \quad (1)$$

where γ is the band parameter, $\hat{\mathbf{k}} = (\hat{k}_x, \hat{k}_y)$ is a wave-vector operator, ε is the energy, and $\vec{\sigma} = (\sigma_x, \sigma_y)$ with σ_x and σ_y being the Pauli spin matrices. Equation (1) has the form of Weyl's equation for neutrinos, i.e., relativistic electrons with vanishing rest mass.

The electronic states can be obtained by imposing the periodic boundary condition in the circumference direction $\Psi(\mathbf{r} + \mathbf{L}) = \Psi(\mathbf{r})$ except for extremely thin CNs. The Bloch functions at a K point change their phase by $\exp(i\mathbf{K} \cdot \mathbf{L}) = \exp(2\pi i\nu/3)$, where ν is an integer defined by $n_a + n_b = 3M + \nu$ with integer M and can take 0 and ± 1 . Because $\Psi(\mathbf{r})$ is written as a product of the Bloch function and the envelope function, this phase change should be canceled by that of the envelope functions and the boundary conditions for the envelope functions are given by $\mathbf{F}^K(\mathbf{r} + \mathbf{L}) = \mathbf{F}^K(\mathbf{r}) \exp(-2\pi i\nu/3)$. The extra phase can be regarded as a fictitious Aharonov-Bohm flux passing through the cross section of CN.

Energy levels in CN for the K point are obtained by putting $k_x = \kappa_\nu(n)$ with $\kappa_\nu(n) = (2\pi/L)[n - (\nu/3)]$ and $k_y = k$ in the above $\mathbf{k} \cdot \mathbf{p}$ equation as $\varepsilon_\nu^{(\pm)}(n, k) = \pm \gamma \sqrt{\kappa_\nu(n)^2 + k^2}$ [11], where $L = |\mathbf{L}|$, n is an integer, and the upper (+) and lower (-) signs represent the conduction and valence bands, respectively. The Hamiltonian for $\mathbf{F}^{K'}$ for the K' point is obtained by replacing \hat{k}_y by $-\hat{k}_y$ or \hat{k}_x by $-\hat{k}_x$ and therefore the corresponding energy levels are obtained by replacing ν by $-\nu$. This shows that CN becomes metallic for $\nu = 0$ and semiconducting with gap $E_g = 4\pi\gamma/3L$ for $\nu = \pm 1$.

3. Optical absorption, band gaps, and excitons

3.1. Polarization and selection rules

The optical absorption is described by a dynamical conductivity obtained in a linear response theory [23]. We first expand electric field $E_\alpha(\theta, \omega)$ and induced current density $j_\alpha(\theta, \omega)$ into a Fourier series:

$$E_\alpha(\theta, \omega) = \sum_l E_\alpha^l(\omega) \exp(il\theta - i\omega t), \quad j_\alpha(\theta, \omega) = \sum_l j_\alpha^l(\omega) \exp(il\theta - i\omega t), \quad (2)$$

with $\alpha = x, y$ and $\theta = 2\pi x/L$. It is quite straightforward to show that the induced current has the same Fourier component as that of the electric field, i.e., $j_\alpha^l(\omega) = \sigma_{\alpha\alpha}^l(\omega) E_\alpha^l(\omega)$. The dynamical conductivity is given by

$$\sigma_{\alpha\alpha}^l(\omega) = \sum_{nk} \frac{|(n, k, +|j_\alpha^l|n+l, k, -)|^2}{iLA[\varepsilon_n^{(+)}(k) - \varepsilon_{n+l}^{(-)}(k)]} \frac{f[\varepsilon_{n+l}^{(-)}(k)](1 - f[\varepsilon_n^{(+)}(k)])2\hbar^2\omega}{[\varepsilon_n^{(+)}(k) - \varepsilon_{n+l}^{(-)}(k)]^2 - (\hbar\omega)^2 - i\hbar^2\omega/\tau}, \quad (3)$$

where A is the length of the nanotube, the current-density operator is given by $j_\alpha^l = -(e\gamma/\hbar)\sigma_\alpha e^{-il\theta}$, a phenomenological relaxation time τ has been introduced, and $f(\varepsilon)$ is the Fermi distribution function.

When external electric field \mathbf{D} is polarized along the CN axis, the Fourier components of a total field are $E_y^l = D_y \delta_{l,0}$ and the absorption is proportional to $\text{Re}\sigma_{yy}(\omega)$ with $\sigma_{yy}(\omega) = \sigma_{yy}^{l=0}(\omega)$. It can be seen from eq. (3) that transitions occur between valence and conduction bands with the same band index n . At a band edge $k=0$, in particular, the envelope function is given by an eigenvector of a Pauli matrix σ_x . Because the current operator j_y is proportional to σ_y , the transitions at their edges are all allowed.

The situation becomes much more complicated when an external electric field is polarized in the direction perpendicular to the CN axis. In this case, effects of an electric field induced by the polarization of nanotubes should be considered. This depolarization effect can be calculated also in the $\mathbf{k} \cdot \mathbf{p}$ scheme.

Suppose an external electric field $D_x^l e^{il\theta - i\omega t}$ is applied in the direction normal to the tube axis and let j_x^l be the induced current. Then, the corresponding induced charge density localized on the cylindrical surface is calculated as $\rho^l = (2\pi/L)(l/\omega)j_x^l$ with the use of the equation of continuity. This charge leads to potential $\phi^l = (L/\kappa|l|)\rho^l$ or electric field $E_x^l = -i(2\pi/\kappa L)l\phi^l$. The static dielectric constant κ describes polarization of states (σ and π bands) except those lying in the vicinity of the Fermi level. It is expected to be in the range $1 < \kappa < 10$, but its exact value is not known. Thus, the total electric field becomes $E_x^l = D^l - i|l|(4\pi^2/\kappa L\omega)j_x^l$, which leads with the use of $j_x^l = \sigma_{xx}^l E_x^l$ to $j_x^l = \tilde{\sigma}_{xx}^l D_x^l$, where

$$\tilde{\sigma}_{xx}^l = \sigma_{xx}^l \left(1 + i|l| \frac{4\pi^2}{\kappa L\omega} \sigma_{xx}^l\right)^{-1}. \quad (4)$$

For the light-polarization perpendicular to the tube axis, its field is written as $\mathbf{D} = (D_x \sin \theta, 0)$. The absorption in a unit area is then proportional to $\text{Re}(j_x E_x^*) \propto \text{Re}\tilde{\sigma}_{xx}(\omega)$ with $\tilde{\sigma}_{xx} = \tilde{\sigma}_{xx}^{l=1} = \tilde{\sigma}_{xx}^{l=-1}$. According to eq. (3) the absorption occurs between the valence band with index n and the conduction bands with $n \pm 1$.

Let us consider a spectral edge corresponding to $k=0$, for which the eigenstates are those of a Pauli matrix σ_x . Because the current operator is proportional to σ_x , transitions between valence- and conduction-band states become allowed only when $\kappa_{\nu\varphi}(n)$ and $\kappa_{\nu\varphi}(n \pm 1)$ have a sign opposite to each other. This leads to the conclusion in a metallic CN, for example, that transitions from $n=0$ to $n=-1$ and from $n=-1$ to $n=0$ are allowed as shown in Fig. 2. When the depolarization effect is included, however, these peaks disappear almost completely because most of their intensity is transferred to interband plasmons [23].

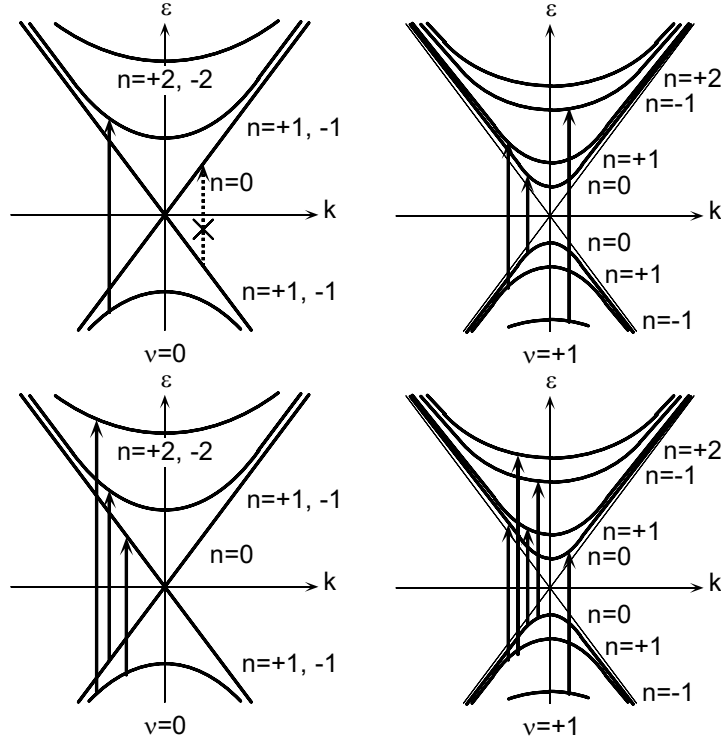


Figure 2. The band structures of a metallic ($\nu = 0$) and semiconducting CN ($\nu = +1$). The allowed optical transitions for the parallel polarization are denoted by arrows in the upper figure and those for the perpendicular polarization in the lower figure.

Therefore, interband optical transitions among valence and conduction bands near the Fermi level can be observable only for polarization parallel to the tube axis.

3.2. Band gap renormalization and excitons

One important problem is a many-body effect on the band structure and optical absorption spectrum. In fact, band gaps are likely to be influenced strongly by electron-electron interactions. Further, the exciton binding energy becomes infinite in the limit of an ideal one-dimensional electron-hole system [35, 36]. This means that the exciton effect can be quite important and modify the absorption spectra drastically. Such band-gap renormalization and optical spectra with exciton effects have been calculated in the conventional screened Hartree-Fock approximation within a $\mathbf{k}\cdot\mathbf{p}$ scheme [24].

The strength of the Coulomb interaction is specified by $(e^2/\kappa L)/(2\pi\gamma/L)$, which turns out to be independent of the circumference length L . In the $\mathbf{k}\cdot\mathbf{p}$ scheme, therefore, all physical quantities become almost universal if the length is scaled by L and the energy by $2\pi\gamma/L$. This parameter is estimated as $(e^2/\kappa L)(2\pi\gamma/L)^{-1} = 0.3545 \times \kappa^{-1}$ for $\gamma = \sqrt{3}a|\gamma_0|/2$ with $\gamma_0 = 3.03$ eV, where $-\gamma_0$ is the transfer integral between nearest-neighbor carbon atoms.

Figure 3 shows some examples of calculated exciton energy levels for a semiconducting CN ($\nu = 1$) versus the strength of the Coulomb interaction. With the increase of the interaction, the number of exciton bound states increases and their energy levels are shifted to the higher energy side in spite of the fact that their binding energy increases. The reason is in the considerable enhancement of the band gap due to the Coulomb interaction. It is interesting to notice that the energy of the lowest excitonic state varies very little as a function of the

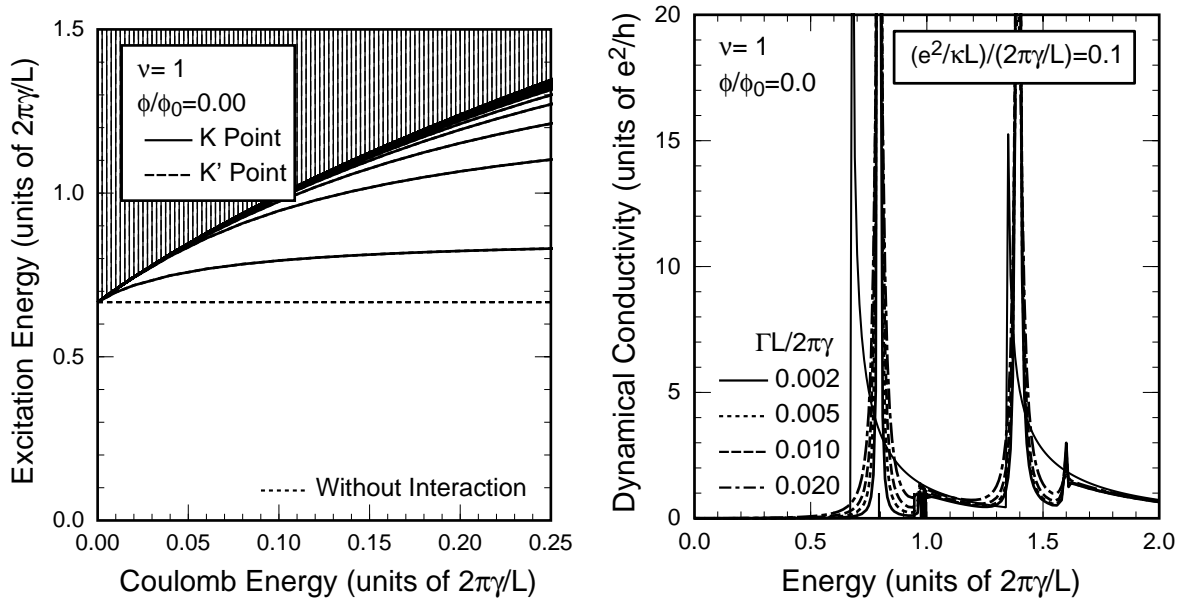


Figure 3. Interband excitation spectra calculated in a screened Hartree-Fock approximation (left) and examples of interband optical absorption spectra in the presence of electron-electron interaction (right).

strength of the Coulomb interaction.

Figure 3 shows calculated absorption spectra in a semiconducting CN for $(e^2/\kappa L)/(2\pi\gamma/L) = 0.1$. The energy levels of excitons are denoted by vertical straight lines. The considerable optical intensity is transferred to the lowest exciton bound states. For a sufficiently larger strength of the Coulomb interaction, transitions to exciton excited states become appreciable.

In addition to excitons associated with the highest valence and the lowest conduction bands ($n=0$), exciton effects are important for transitions to excited bands. In fact, the exciton binding energy and the intensity transfer is larger for the transition to the higher conduction band ($n=1$) than those with $n=0$. This arises because the effective mass along the axis direction for the conduction and valence bands with $n=1$ is twice as large as that of the lowest conduction band and the highest valence band with $n=0$.

It turned out that interaction effects on the band gap are almost independent of $n=0$ and $n=1$ and the exciton energy is almost as large as the band-gap renormalization for the bands with larger optical gap $n=1$. As a result, the absorption peak stays almost at the corresponding band gap in the absence of interaction and exciton effects for $n=1$ and the energy difference between the absorption peaks for $n=0$ and $n=1$ becomes smaller than that in the absence of interactions.

Optical absorption spectra of thin film samples of single-wall nanotubes were observed quite recently and analyzed by assuming a distribution of their chirality and diameter [37]. Careful comparison of the observed spectrum with calculated in a simple tight-binding model suggested the importance of excitonic effects [38]. In fact, comparing the observed spectrum with the calculated one in the fundamental absorption region, the observed absorption band for $n=0$ lies at an energy higher than half of the band for $n=1$. The results can roughly be explained by the theoretical result for $(e^2/\kappa L)/(2\pi\gamma/L) \sim 0.05$. This result strongly suggests that the exciton effect together with the band-gap renormalization plays an important role in the optical transition near the fundamental absorption edge in semiconducting nanotubes.

4. Absence of Backward Scattering

4.1. Berry's phase and topological singularity

The wave function is written explicitly as

$$\mathbf{F}_{s\mathbf{k}} = \frac{1}{\sqrt{2}} \begin{pmatrix} e^{i\theta(\mathbf{k})} \\ s \end{pmatrix} \frac{1}{\sqrt{LA}} \exp(i\mathbf{k} \cdot \mathbf{r}), \quad (5)$$

where $\theta(\mathbf{k})$ is the direction angle of \mathbf{k} , $s = +1$ and -1 for the conduction and valence band, respectively, and A is the CN length. This wave function acquires Berry's phase $-\pi$ when the wave vector \mathbf{k} is rotated around the origin $\mathbf{k} = 0$, although it looks continuous as a function of \mathbf{k} [18, 39]. In fact, when \mathbf{k} is rotated once in the anticlockwise direction adiabatically as a function of time t for a time interval $0 < t < T$ with $\mathbf{k}(T) = \mathbf{k}(0)$, the wavefunction $\mathbf{F}_{s\mathbf{k}}$ is changed into $\mathbf{F}_{s\mathbf{k}} \exp(-i\varphi)$, where φ is Berry's phase given by

$$\varphi = -i \int_0^T dt \left\langle s\mathbf{k}(t) \left| \frac{d}{dt} \right| s\mathbf{k}(t) \right\rangle = -\pi. \quad (6)$$

This is equivalent to the well-known signature change of the spinor wave function or a spin rotation operator under a 2π rotation.

It should be noted that $\varphi = -\pi$ when the closed contour encircles the origin $\mathbf{k} = 0$ but $\varphi = 0$ when the contour does not contain $\mathbf{k} = 0$. Further, the wave function at $\mathbf{k} = 0$ depends on the direction of \mathbf{k} and its "spin" direction is undefined. These facts show the presence of a topological singularity at $\mathbf{k} = 0$. The nontrivial Berry's phase leads to the unique property of a metallic carbon nanotube that there exists no backscattering and the tube is a perfect conductor even in the presence of scatterers [17, 18]. In fact, it has been proved that the Born series for backscattering vanish identically and the conductance calculated exactly for finite-length nanotubes containing many impurities is given by $2e^2/\pi\hbar$ independent of length [17]. The absence of backscattering has been confirmed also by numerical calculations in a tight binding model [19].

Backscattering corresponds to a rotation of the \mathbf{k} direction by $\pm\pi$. In the absence of a magnetic field, there exists a time reversal process corresponding to each backscattering. This process corresponds to a rotation by $\pm\pi$ in the opposite direction. The scattering amplitudes of these two processes are same in the absolute value but have opposite signatures because of Berry's phase. As a result, the backscattering amplitude cancels out completely. In semiconducting nanotubes, on the other hand, backscattering appears because the symmetry is destroyed by a nonzero Aharonov-Bohm magnetic flux.

An important information has been obtained on the effective mean free path in nanotubes by single-electron tunneling experiments [40, 41]. The Coulomb oscillation in semiconducting nanotubes is quite irregular and can be explained only if nanotubes are divided into many separate spatial regions in contrast to that in metallic nanotubes [20]. This behavior is consistent with the presence of considerable amount of backward scattering leading to a strong localization of the wave function. In metallic nanotubes, the wave function is extended in the whole region of a nanotube because of the absence of backward scattering. With the use of electrostatic force microscopy the voltage drop in a metallic nanotube has been shown to be negligible in comparison with an applied voltage [21].

4.2. Phonons and electron-phonon scattering

At nonzero temperatures, lattice vibrations usually constitute the major source of electron scattering and limit the resistivity. Usually long-wavelength acoustic phonons are most important. These modes can be described by a continuum model [42, 43, 44]. An acoustic

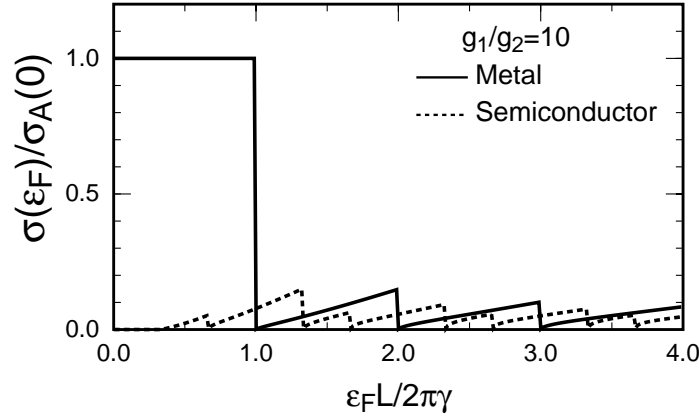


Figure 4. The Fermi-energy dependence of the conductivity for metallic (solid line) and semiconducting (broken line) CNs with $g_1/g_2=10$ in units of $\sigma_A(0)$ denoting the conductivity of an armchair CN with $\epsilon_F=0$. After Ref. [44].

phonon gives rise to an effective electron-phonon coupling called the deformation potential $V_1 = g_1(u_{xx} + u_{yy})$ with $u_{xx} = (\partial u_x / \partial x) + (u_z / R)$ and $u_{yy} = \partial u_y / \partial y$, where u_x , u_y , and u_z represent lattice displacements in the x , y , and z directions, respectively, and R is the CN radius. This potential appears as a diagonal term. A very rough estimation gives $g_1 \sim 30$ eV.

A phonon causes also a change in the distance between neighboring carbon atoms. This gives rise to an off-diagonal term $V_2 = g_2 e^{3i\eta} (u_{xx} - u_{yy} + 2iu_{xy})$ with $g_2 = (3\alpha\beta/4)\gamma_0$, where $\beta = -d \ln \gamma_0 / d \ln b$, b is the bond length, and α is a quantity smaller than unity dependent on microscopic models of phonons. Usually, we have $\beta \sim 2$ [45] and $\alpha \sim 1/3$, which give $g_2 \sim \gamma_0/2$ or $g_2 \sim 1.5$ eV. This coupling constant is more than one order of magnitude smaller than the deformation potential. It corresponds to one given previously [46] without the reduction factor α .

The diagonal terms do not contribute to the backscattering as in the case of impurities and only the much smaller off-diagonal terms have some contribution. The mean free path Λ is estimated as $\Lambda = (\mu a^2 / 3k_B T \alpha^2 \beta^2) L$, where $L = |\mathbf{L}|$, μ is the shear modulus of 2D graphite, and a is the lattice constant. We obtain $\Lambda \sim 600L$ at room temperature, which is larger than $1 \mu\text{m}$ for thin armchair nanotubes with diameter ~ 1.5 nm and increases in proportion to L with L . This shows that a metallic CN is ballistic even at room temperature. The situation changes dramatically when other bands start to be occupied. Figure 4 shows the Fermi energy dependence of the conductivity obtained by solving Boltzmann equation [44].

5. Summary and Conclusion

In summary, an electron in a nanotube is a neutrino on a cylinder surface with a fictitious Aharonov-Bohm flux. Optical absorptions are appreciable only for polarization parallel to the axis and affected by interactions and excitonic effects. A topological singularity gives rise to the absence of backscattering except for scatterers with a range smaller than the lattice constant and a metallic nanotube becomes a ballistic conductor even at room temperature.

Acknowledgements

This work has been supported in part by Grants-in-Aid for COE (12CE2004 “Control of Electrons by Quantum Dot Structures and Its Application to Advanced Electronics”) and

Scientific Research from the Ministry of Education, Culture, Sports, Science and Technology, Japan.

References

- [1] Iijima S 1991 *Nature* (London) 354 56
- [2] Hamada N, Sawada S and Oshiyama A 1992 *Phys. Rev. Lett.* 68 1579
- [3] Mintmire J W, Dunlap B I and White C T 1992 *Phys. Rev. Lett.* 68 631
- [4] Saito R, Fujita M, Dresselhaus G and Dresselhaus M S 1992 *Phys. Rev. B* 46 1804; 1992 *Appl. Phys. Lett.* 60 2204
- [5] Dresselhaus M S, Dresselhaus G and Saito R 1992 *Phys. Rev. B* 45 6234
- [6] Jishi R A, Dresselhaus M S and Dresselhaus G 1993 *Phys. Rev. B* 47 16671
- [7] Tanaka K, Okahara K, Okada M and Yamabe T 1992 *Chem. Phys. Lett.* 191 469
- [8] Gao Y D and Herndon W C 1992 *Mol. Phys.* 77 585
- [9] Robertson D H, Brenner D W and Mintmire J W 1992 *Phys. Rev. B* 45 12592
- [10] White C T, Robertson D C and Mintmire J W 1993 *Phys. Rev. B* 47 5485
- [11] Ajiki H and Ando T 1993 *J. Phys. Soc. Jpn.* 62 1255
- [12] Rao A M, Richter E, Bandow S, Chase B, Eklund P C, Williams K W, Menon M, Subbaswamy K R, Thess A, Smalley R E, Dresselhaus G and Dresselhaus M S 1997 *Science* 275 187
- [13] Olk C H and Heremans J P 1995 *J. Mater. Res.* 9 259
- [14] Wildoer J W, Venema L C, Rinzler A G, Smalley R E and Dekker C 1998 *Nature* (London) 391 59
- [15] Hassanien A, Tokumoto M, Kumazawa Y, Kataura H, Maniwa Y, Suzuki S and Achiba Y 1998 *Appl. Phys. Lett.* 73 3839
- [16] Ando T 2000 *Semicond. Sci. Technol.* 15 R13
- [17] Ando T and Nakanishi T 1998 *J. Phys. Soc. Jpn.* 67 1704
- [18] Ando T, Nakanishi T and Saito R 1998 *J. Phys. Soc. Jpn.* 67 2857
- [19] Nakanishi T and Ando T 1999 *J. Phys. Soc. Jpn.* 68 561
- [20] McEuen P L, Bockrath M, Cobden D H, Yoon Y -G and Louie S G 1999 *Phys. Rev. Lett.* 83 5098
- [21] Bachtold A, Fuhrer M S, Plyasunov S, Forero M, Anderson E H, Zettl A and McEuen P L 2000 *Phys. Rev. Lett.* 84 6082
- [22] Ajiki H and Ando T 1993 *J. Phys. Soc. Jpn.* 62 2470 [Errata 1994 *J. Phys. Soc. Jpn.* 63 4267]
- [23] Ajiki H and Ando T 1994 *Physica B* 201 349; 1995 *Jpn. J. Appl. Phys. Suppl.* 34-1 107
- [24] Ando T 1997 *J. Phys. Soc. Jpn.* 66 1066
- [25] Viet N A, Ajiki H and Ando T 1994 *J. Phys. Soc. Jpn.* 63 3036
- [26] Suzuura H and Ando T 2001 *Proceedings of 25th International Conference on the Physics of Semiconductors*, edited by Miura N and Ando T (Springer, Berlin, 2001), p. 1525
- [27] Ajiki H and Ando T 1995 *J. Phys. Soc. Jpn.* 64 260; 1996 *J. Phys. Soc. Jpn.* 65 2976
- [28] Ajiki H and Ando T 1995 *J. Phys. Soc. Jpn.* 64 4382
- [29] Ando T 2000 *J. Phys. Soc. Jpn.* 69 1757
- [30] Ando T, Nakanishi T and Igami M 1999 *J. Phys. Soc. Jpn.* 68 3994
- [31] Igami M, Nakanishi T and Ando T 2001 *J. Phys. Soc. Jpn.* 70 481
- [32] Yaguchi T and Ando T 2001 *J. Phys. Soc. Jpn.* 70 3641; 2002 *J. Phys. Soc. Jpn.* (in press)
- [33] Wallace P R 1947 *Phys. Rev.* 71 622
- [34] Slonczewski J C and Weiss P R 1958 *Phys. Rev.* 109 272
- [35] Loudon R 1959 *Am. J. Phys.* 27 649
- [36] Elliot R J and Loudon R 1959 *J. Phys. Chem. Solids* 8 382; 1960 *J. Phys. Chem. Solids* 15 196
- [37] Kataura H, Kumazawa Y, Maniwa Y, Umezū I, Suzuki S, Ohtsuka Y and Achiba Y 1999 *Synth. Met.* 103 2555
- [38] Ichida M, Mizuno S, Tani Y, Saito Y and Nakamura A 1999 *J. Phys. Soc. Jpn.* 68 3131
- [39] Berry M V 1984 *Proc. Roy. Soc. London A* 392 45
- [40] Tans S J, Devoret M H, Dai H, Thess A, Smalley R E, Geerligs L J and Dekker C 1997 *Nature* (London) 386 474
- [41] Bezryadin A, Verschueren A R M, Tans S J and Dekker C 1998 *Phys. Rev. Lett.* 80 4036
- [42] Suzuura H and Ando T 2000 *Physica E* 6 864
- [43] Suzuura H and Ando T 2000 *Mol. Cryst. Liq. Cryst.* 340 731
- [44] Suzuura H and Ando T 2002 *Phys. Rev. B* 65 235412
- [45] See for example, Harrison W A 1980 *Electronic Structure and the Properties of Solids* (W.H. Freeman and Company, San Francisco, 1980).
- [46] Kane C L and Mele E J 1987 *Phys. Rev. Lett.* 78 1932